7.11 EVALUATION OF TURBULENCE MODELS FOR LARGE-EDDY SIMULATIONS OF FLOW OVER ASKERVEIN HILL

Fotini Katopodes Chow* and Robert L. Street
Environmental Fluid Mechanics Laboratory, Stanford University, Stanford, California

1. INTRODUCTION AND BACKGROUND

The evaluation of turbulence closure models for large-eddy simulation (LES) has primarily been performed over flat terrain, where comparisons to theory and observations are simplified. We previously successfully demonstrated the performance of explicit filtering and reconstruction turbulence modeling for flat neutral boundary layer flows (Chow, 2004). We now turn to a more challenging test case, flow over a hill, that includes the effects of terrain. Our modeling approach, called the dynamic reconstruction model (DRM), uses series expansions for reconstruction of the resolvable subfilter-scale (RSFS) stresses together with the dynamic eddy viscosity model of Wong and Lilly (1994) for the subgrid-scale (SGS) stresses. This is the first time, to our knowledge, that either reconstruction (scale-similarity) or dynamic turbulence models have been applied to full-scale simulations of the atmospheric boundary layer over terrain.

Several studies have been performed over simple hills to evaluate the performance of different turbulence models; however, most are done at laboratory scales because of the availability of experimental data for comparison (Brown et al., 2001; Allen and Brown, 2002; Besio et al., 2003). Such simulations are convenient because they have clearly defined boundary conditions and are generally well-resolved numerically because of the low Reynolds number conditions.

As our interest is in improving the performance of mesoscale atmospheric flow simulations, we have instead chosen to simulate flow over Askervein hill, a relatively isolated hill located along the west coast of South Uist island, Scotland. The Askervein hill project (Taylor and Teunissen, 1987) collected velocity and turbulence data that provide a unique dataset for comparison to numerical simulations. Similar observational datasets are also available from field campaigns performed at Black Mountain (Bradley, 1980), Cinder Cone Butte (Lavery et al., 1982; Strimaitis et al., 1982), Blashaval hill (Mason and King, 1985), and Kettles hill (Salmon et al., 1988), among others. We selected Askervein hill because turbulence measurements are available for comparison and because this flow has been extensively modeled by other researchers (Raithby et al., 1987; Kim and Patel, 2000; Castro et al., 2003). The goal of this work is to evaluate the new turbulence closure methods presented by Chow et al. (2004) for flow over terrain.

2. MODEL SETUP

We follow the examples given by Raithby et al. (1987) and Castro et al. (2003), and compare our simulation results to field measurements TU-03a, TU-03b, MF-03d and TK03 of Taylor and Teunissen (1985), collected between 1200 and 1700 (British summer time = UTC + 1 hour) on October 3, 1983. These observation periods had Richardson numbers between -0.0038 and -0.011 (very slightly unstable), therefore the atmosphere can be considered approximately neutrally stratified. The moderate to strong winds (e.g. 10 m/s wind speed at the reference site (see RS in Fig. 1) at 10 m above ground level for TU-03a and 8.9 m/s for TU-03b) were fairly steady (from the southwest, 210° clockwise from North) during this time period. Intermittent separation was observed in the lee of the hill. A long rain shower occurred earlier in the morning, and low clouds were present at approximately 300 m above ground level (agl) (at less than 300 m agl over the hills). This perhaps indicates the presence of a stable layer at about 300 m. The observed mean flow data were averaged in time over 10 minutes and turbulence data were calculated over 30 minutes (Taylor and Teunissen, 1987).

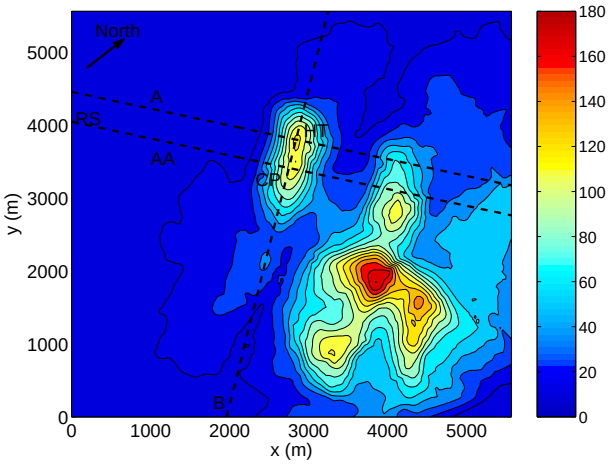

Figure 1: Elevation contours (m) used in simulation, rotated 60 degrees clockwise from north. Contour interval is 12 m.

For our simulations, we use the Advanced Regional Prediction System (ARPS), developed at the Center for Analysis and Prediction of Storms at the University of Oklahoma. Intended mainly for mesoscale and small-scale atmospheric simulations, ARPS is formulated as an LES code and solves the three-dimensional, compressible, non-hydrostatic, filtered Navier-Stokes equations. Details can be found in Xue et al. (1995, 2000, 2001).

Topographic data for Askervein were provided by Walmsley and Taylor (1996) at approximately 25 m horizontal resolution. Elevation contours are shown in Fig. 1. The grid (centered near Askervein hill, 57° 11' N, -7° 22'

*Corresponding author address: Environmental Fluid Mechanics Laboratory, Department of Civil and Environmental Engineering, Stanford University, Terman Engineering Center M-13, Stanford, CA 94305-4020, email: katopodes @ stanfordalumni.org

W) was rotated 60 degrees clockwise to align the y-axis with the incoming 210°N winds. Elevations were interpolated to 35 m horizontal resolution using 163 × 163 grid points to cover a 5600 m square domain. In the vertical, 59 points are used; the minimum grid spacing is 5 m at the ground surface and is stretched using a tanh function to yield an averaging spacing of 12.5 m over the 700 m vertical extent of the domain. This grid configuration provides the combination of low grid aspect ratio and high-resolution required for accurate large-eddy simulations. Simulations were also performed with a 1000 m domain height, but with very little difference in the results, so they are not shown.

We use a roughness value of z_0 = 0.03 m and apply a log-law bottom boundary condition as done by both Raithby et al. (1987) and Castro et al. (2003). The flow is allowed to spin up for 2700 s, after which 900 s of data are collected for averaging at 30 s intervals. For the turbulence statistics, 1800 s of data are collected.

Reference simulations were performed using the standard 1.5-order TKE closure (Deardorff, 1980; Moeng, 1984) in ARPS. These are compared to results from the dynamic Wong-Lilly (DWL) (Wong and Lilly, 1994) and the dynamic reconstruction (DRM) models (Gullbrand and Chow, 2003; Chow, 2004). The DWL is written

$$\tau_{ij} = -2C_\epsilon \Delta^{4/3} \overline{\tilde{S}}_{ij} \ , \qquad (1)$$

where τ_{ij} is the total subfilter-scale (SFS) stress, S_{ij} is the strain rate, Δ is the filter width, and the overbar indicates a spatial filter and the tilde the discretization operator (see Gullbrand and Chow, 2003). The coefficient C_ϵ is determined dynamically. The DRM is a mixed model for the total SFS stress consisting of scale-similarity and eddy-viscosity terms:

$$\tau_{ij} = \left(\overline{\tilde{u}_i^\star \tilde{u}_j^\star} - \overline{\tilde{u}_i^\star}\,\overline{\tilde{u}_j^\star} \right) - 2C_\epsilon \Delta^{4/3} \overline{\tilde{S}}_{ij} \ . \qquad (2)$$

Reconstruction using the van Cittert iterative series expansion method (from the approximate deconvolution method (ADM) of Stolz et al. (2001)) provides an estimate ($\tilde{u}_i^\star$) of the unfiltered velocity (u_i) in terms of the filtered velocity ($\overline{\tilde{u}}_i$); this is used to calculate the RSFS stresses (the first pair of terms in Eq. 2). The eddy-viscosity (the last term) contribution is provided by the Wong-Lilly model. The level of reconstruction (n) is determined by the number of terms ($n+1$) in the series expansion; for example, level-0 reconstruction includes one term in the series and is denoted DRM-ADM0. When the DWL is used alone, the contribution of the RSFS terms is ignored. As discussed in Section 4, reconstruction of levels greater than zero leads to terrain-induced instabilities. Modifications are proposed to allow for higher levels of reconstruction.

To provide a realistic turbulent inflow, a separate neutral boundary layer simulation with periodic boundary conditions and flat terrain is performed and data are extracted from a vertical yz-slice in the domain at every time step. This "turbulence database" is based on the simulations performed in Chow (2004) using the level-0 dynamic reconstruction closure model (DRM-ADM0), which provides a good representation of the logarithmic velocity profile expected in a neutral boundary layer. The grid size for this periodic case is (83,163,83) with 35 m horizontal and 5 m minimum vertical resolution, covering a 2800 × 5600 × 1000 m domain. The 1000 m domain height also accommodated the grids of different vertical extent which were tested for the Askervein grid. The reference elevation for ARPS is set to 10 m above sea level (asl) so that the pressure matches that at the inflow to the Askervein domain. This turbulent dataset is then used to specify the inflow velocity at every time step on the western side of the Askervein domain. The flow throughout the Askervein domain is thus fully turbulent (see e.g. Fig. 7 later). In contrast, if the flow is driven by constant inflow boundary conditions, it is not able to become fully turbulent over the short length of the domain.

The initial conditions are set to a constant logarithmic velocity profile and neutral stratification. Severe oscillations were initially observed when the turbulent inflow data were imposed, because disturbances at the boundary propagated quickly through the pressure field into the initially uniform flow fields. This was corrected by using the pressure detrending option in ARPS, which sets the domain-wide mean perturbation Exner function to zero to control pressure drift (usually due to boundary condition effects). The effects of the detrending on the flow solution are small; the magnitude of the pressure appears only in the relatively small pressure perturbation contribution to the buoyancy term (Klemp and Wilhelmson, 1978; Xue et al., 1995).

3. COMPARISON WITH OBSERVATIONS

3.1 Mean winds

Observations along lines A and AA (43°, NE-SW) and along line B (133°, SE-NW) in Fig. 1 are compared with the corresponding time-averaged quantities from the three-dimensional simulated velocity fields. Figure 2 shows the wind profile at the reference site (RS), located approximately 2.8 km southsouthwest of the hill top. In our simulations, RS is at the left edge of the domain where it is intersected by line A (instead of by line AA). The observed winds agree well with the logarithmic profile from the turbulent inflow database, which is the same for each simulation.

Figure 3 shows the observed and simulated wind speed-up ratio at 10 m above the ground along lines A and AA. Observation data are not available more than 400 m (line A) or 600 m (line AA) beyond the hill top. The fractional wind speed-up ratio provides the most straightforward comparison of the various model results and is defined as

$$\Delta S = \frac{S(z) - S_{RS}(z)}{S_{RS}(z)} \qquad (3)$$

where S is the horizontal wind speed and S_{RS} is at the reference site. The speed-up is a nondimensional measure often used in wind engineering for siting of wind turbines. All the simulations underpredict the speed-up at the hill top along line A, with the TKE-1.5 results slightly better than the rest. The underprediction at the hill top is likely caused by the fact that the peak elevation is slightly underestimated on our grid (at 122 m, because of the grid spacing) compared to the actual elevation (126 m). The greatest difference among the models is, however, in the lee of the hill, where intermittent separation was observed in the field (Raithby et al., 1987). The TKE-1.5 model fails to produce the observed flow deceleration, whereas the

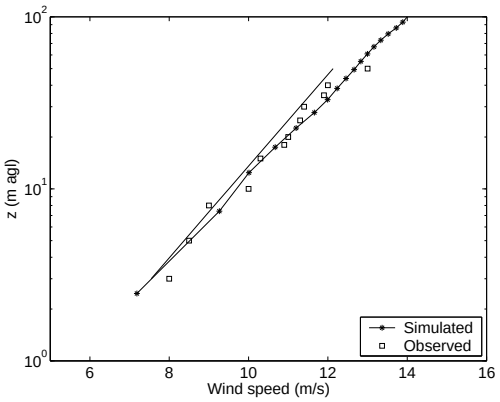

Figure 2: Comparisons of observed wind speed profile at reference site (RS) to simulated values from the turbulent inflow database. A logarithmic profile with $u_* = 0.654$, $z_0 = 0.03$ (as suggested by Raithby et al., 1987) is also shown.

DWL and particularly the DRM-ADM0 results are much better. Similar speed-up results are found along line AA (Fig. 3).

The wind direction deviation from 210° $\Delta\Phi$ is shown in Fig. 4. None of the models completely agrees with the observed wind directions, but the DRM-ADM0 results again show improvement in the lee of the hill.

Fig. 5 shows the wind speedup along line B; here the models slightly overpredict the wind speedup (particularly the TKE-1.5 model) even at the peak of the hill, whereas values were underpredicted in Fig. 3. This may be because of truncation errors in the interpolation procedures used to extract simulation data along lines A and B. Again the general agreement is quite good.

Vertical profiles of the wind speed-up ratio are shown at the hill top (HT) in Figure 6. The speed-up ratio at the hill top is underestimated (as seen in Fig. 3), probably again due in part to the lower hill height in the simulations. The general trend of the speed-up profile is well reproduced by all the turbulence models, with the shape slightly better represented by the dynamic models.

Figures 7 and 8 show instantaneous vertical cross-sections from DRM-ADM0 simulations of the flow over Askervein to illustrate the intermittent separation observed. In Fig. 7 a "gust" event is visible as the winds sweep down the lee side of the hill. This contrasts with Fig. 8, where a separated flow region is observed in the lee of the hill. The recirculation is responsible for the strong deceleration observed in the wind speedup curves (Fig. 3). Clearly, accurate prediction of the intermittent separation is related to the ability to predict the wind speedup. Intermittent separation is a challenge for numerical simulations which are particularly sensitive to the formulations chosen for the wall model and boundary conditions. The TKE-1.5 results did not exhibit these recirculation patterns (not shown), so the speedup ratio is over-predicted (see Fig. 3).

3.1 Turbulence

Comparing turbulent quantities from LES and from observations in the field can be complicated because of the

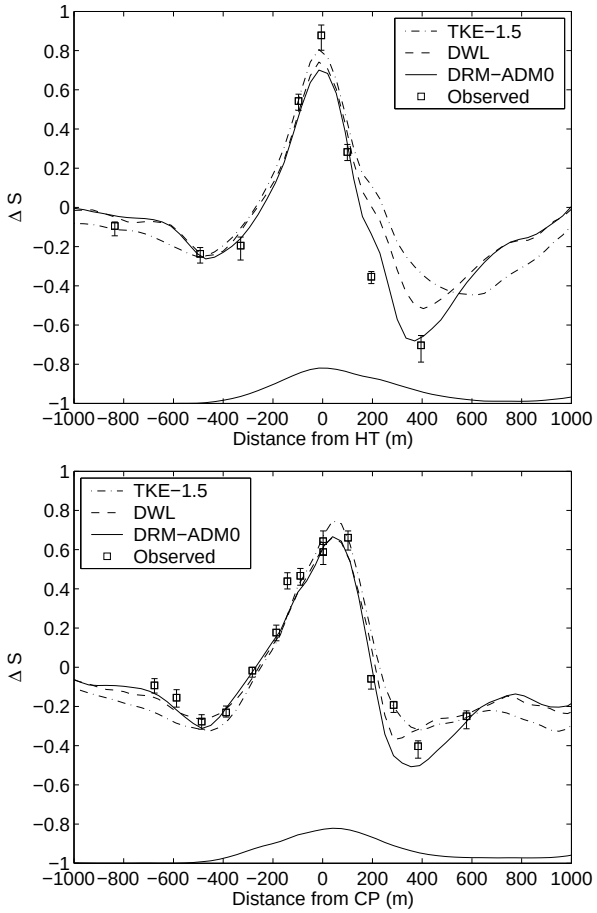

Figure 3: Comparisons of observed velocity speed-up along lines A (top) and AA (bottom) to simulated values using TKE-1.5, DWL and DRM-ADM0 closures. The profile of the hill is shown at the bottom of each axis.

different space and time averaging techniques used. The representation in LES is by definition filtered in space, at least over the dimensions of the grid cell. The measurements in the field are obtained at one specific location and averaged over time. The only option is to attempt to relate the two quantities as best as possible. We define

$$\overline{e}_{ij} \approx \overline{c}_{ij} + < \tau_{ij} > \qquad (4)$$

to calculate the normal stresses and shear stresses, which consists of the familiar resolved ($c_{ij} =< \overline{\overline{u}}_i \overline{\overline{u}}_j > - < \overline{\overline{u}}_i >< \overline{\overline{u}}_j >$) plus subfilter ($\tau_{ij}$) contributions. (The c_{ij} term is filtered here but this does not affect the results much). Time averages (denoted by $<>$) are performed over 30 minutes using LES data at 30 second intervals.

Figure 9 compares computed and observed TKE and uw and vw stresses along line A. The prediction from the DRM-ADM0 is clearly superior to the others for the TKE profiles. Note, however, that the calculation of normal stresses is often difficult because the subgrid model contribution can be difficult to isolate. For example, when using the Smagorinsky model, the normal stresses are quite small because they are absorbed into the pres-

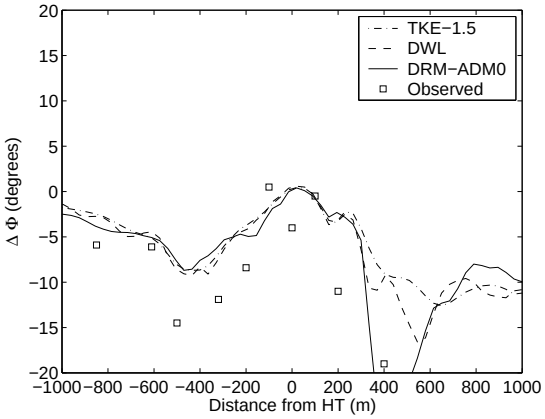

Figure 4: Comparisons of observed wind direction deviation from 210° $\Delta\Phi$ along line A to simulated values using TKE-1.5, DWL and DRM-ADM0 closures.

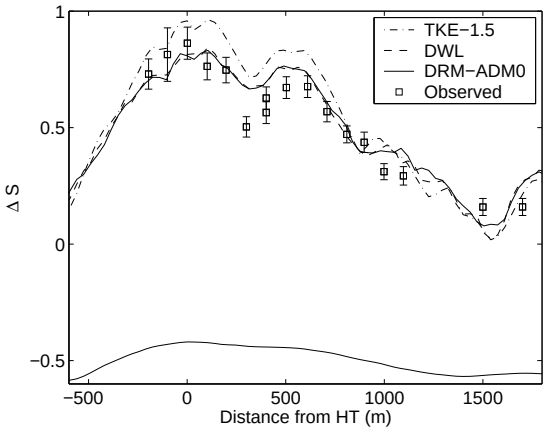

Figure 5: Comparisons of observed velocity speed-up along line B to simulated values using TKE-1.5, DWL and DRM-ADM0 closures. The profile of the hill is shown at the bottom of the figure.

sure term and cannot be recovered (in an incompressible code, the subgrid TKE computed by the Smagorinsky model is identically zero). The uw and vw stresses have been rotated to be aligned with line A. The vw stress comparisons are quite good, but significant differences are observed in the uw plots. The contribution of the subfilter-scale stresses is larger when explicit filtering and reconstruction is used; this is consistent with the results from flow over flat terrain, where the SFS stresses increased with increasing reconstruction, and the resolved stresses decreased accordingly (see Chow, 2004).

4. PERFORMANCE OF THE DYNAMIC RECONSTRUCTION MODELS

The above results for wind speedup and turbulent quantities indicate quite good overall agreement between the observations and the simulations using DWL and especially DRM-ADM0. Attempts to directly increase the level of reconstruction were, however, unsuccessful. Using DRM-ADM1 resulted in instabilities that could only be controlled by increasing the fourth-order computational mixing. This had a strong impact on the velocity profiles near the wall, where gradients are largest; velocities slowed down significantly and wind speedup predictions deteriorated.

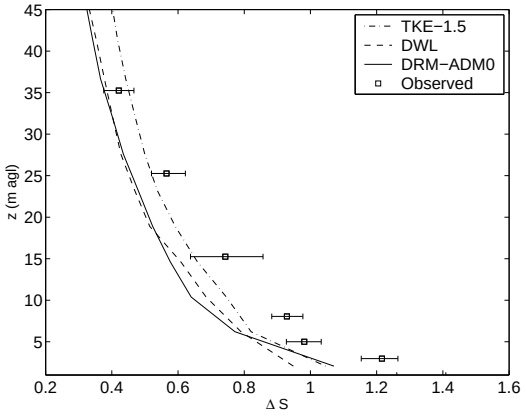

Figure 6: Comparisons of observed velocity speed-up profile at hill top to simulated values using TKE-1.5, DWL and DRM-ADM0 closures.

The performance of the dynamic reconstruction model is very sensitive to the calculation of the dynamic coefficient in the Wong-Lilly model. An indication that the dynamic model struggles with flow over terrain can be seen in Fig. 10, showing contours of the dynamic eddy viscosity. Very near the wall (k = 1), the dynamic coefficient often becomes locally negative, so there is a considerable amount of clipping applied to reset large negative eddy viscosity to -1.5×10^{-5} for stability reasons. Further from the wall (k = 10), the percentage of clipping required is much smaller. Tests using the DWL alone over very complex terrain (see Chow, 2004, Chapter 8) showed very large amounts of clipping and ultimately resulted in instabilities.

Iizuka and Kondo (2003) also had difficulty with the dynamic Smagorinsky model in simulations over a 2D laboratory-scale hill, where the model failed to reproduce the expected recirculation patterns. The authors cited the dynamic model underestimation of the eddy viscosity very near the wall as a key reason for the poor performance of the model over terrain. Given that our full-scale hill terrain is neither smooth, nor two-dimensional, it is not surprising that we experience further difficulties with the dynamic model.

Figure 11 shows sample vertical profiles of the instantaneous and time-averaged eddy viscosity at three locations along line A. The first 5-6 points above the wall exhibit the same pattern observed by Iizuka and Kondo (2003); the eddy viscosity is underpredicted because of difficulties in the dynamic procedure previously cited in neutral boundary layer simulations (Chow et al., 2004; Chow, 2004).

Iizuka and Kondo (2003) proposed a hybrid dynamic-static Smagorinsky model, which uses eddy viscosities from the standard static model at points near the wall

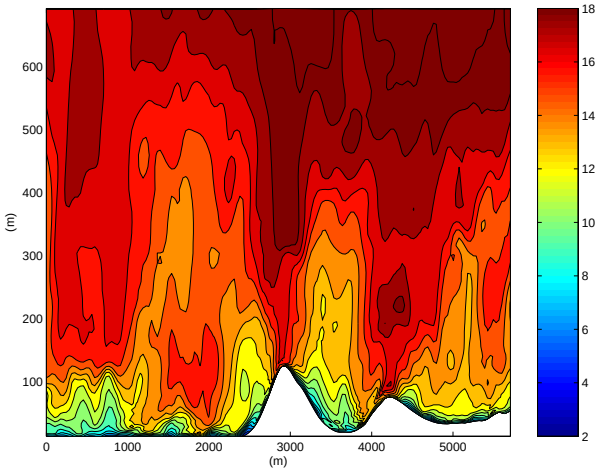

(a)

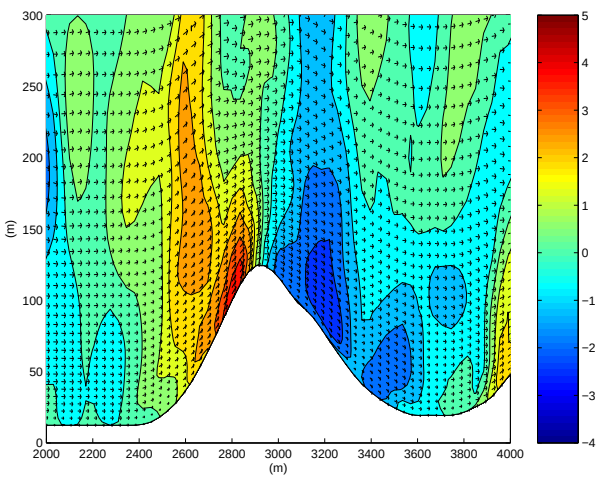

(b)

Figure 7: Vertical cross-section along line A of (a) u-velocity and (b) wind vectors and w-velocity (only a subregion is shown) during a "gust" event, using DRM-ADM0.

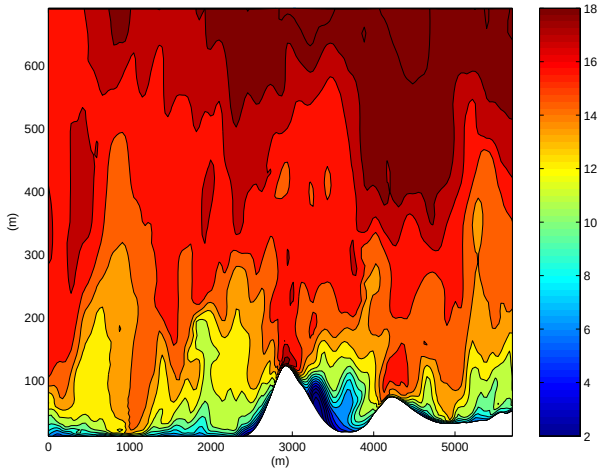

(a)

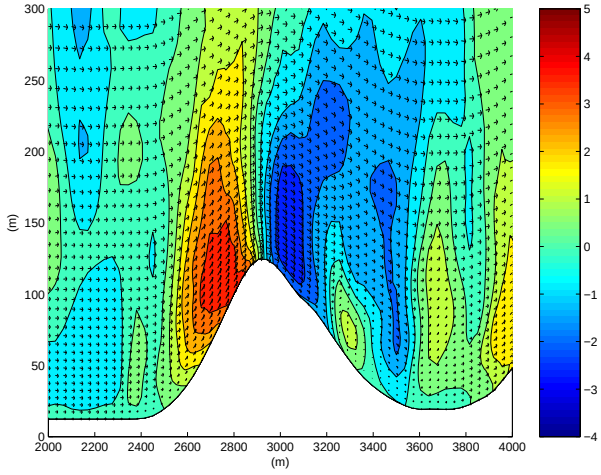

(b)

Figure 8: Vertical cross-section along line A of (a) u-velocity and (b) wind vectors and w-velocity (only a subregion is shown) during a "recirculation" event, using DRM-ADM0.

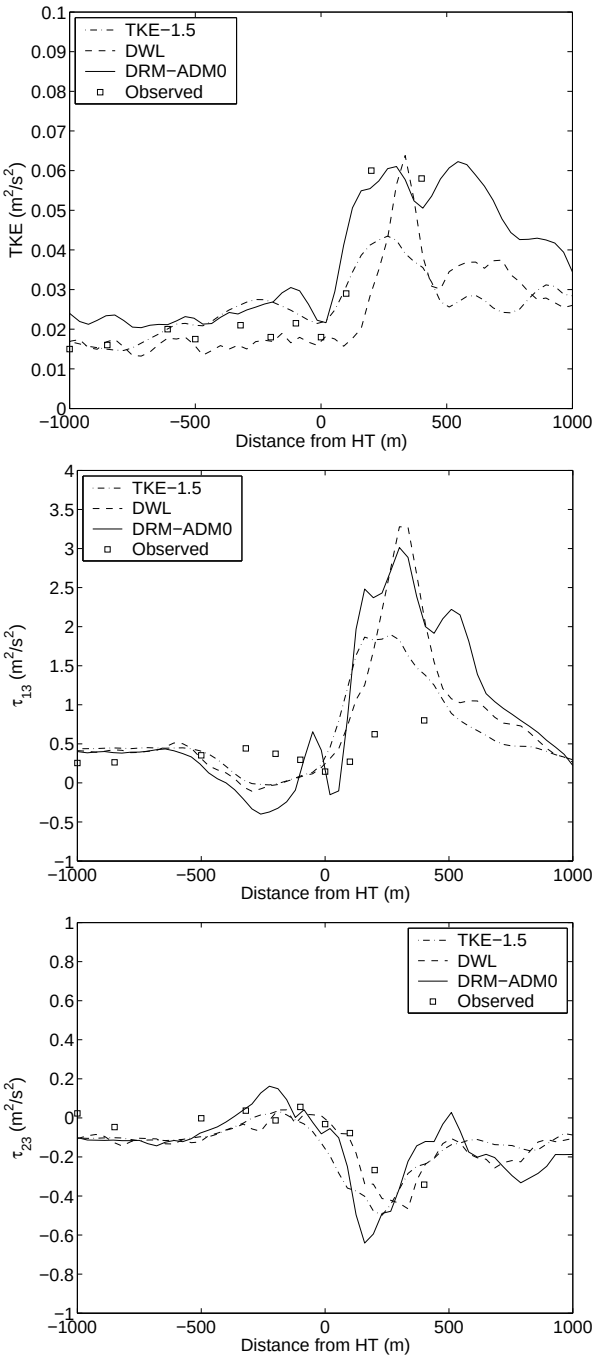

Figure 9: Comparisons of observed TKE (top), uw stress (middle, rotated coordinates), and vw stress (bottom, rotated coordinates) along line A to simulated values using TKE-1.5, DWL and DRM-ADM0 closures.

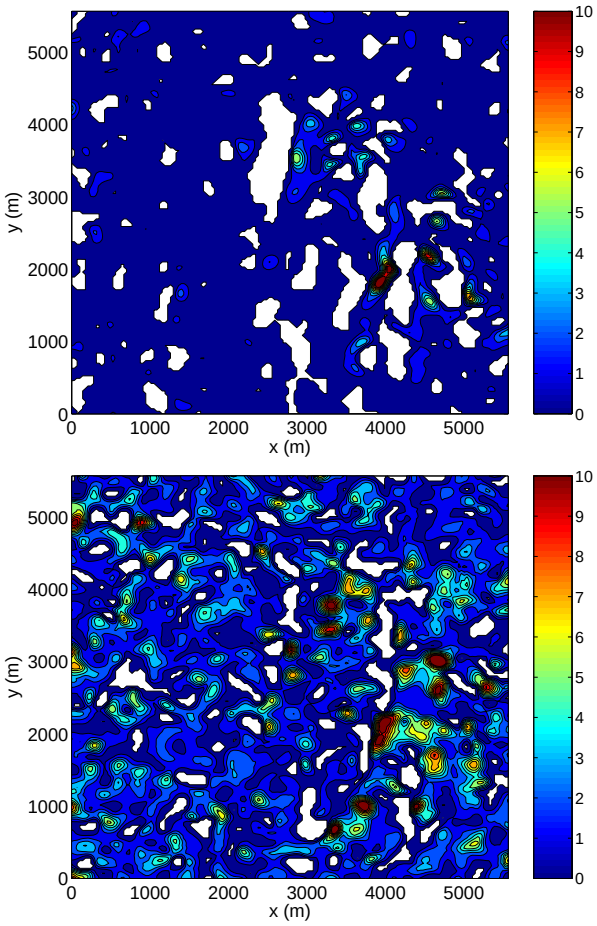

Figure 10: Instantaneous contours of eddy viscosity ν_T (m^2/s) after clipping is applied, for DRM-ADM0 with two local test filters, at k = 1 (top) and k = 10 (bottom). Clipping is indicated by the enclosed white regions with a value of -1.5×10^{-5}.

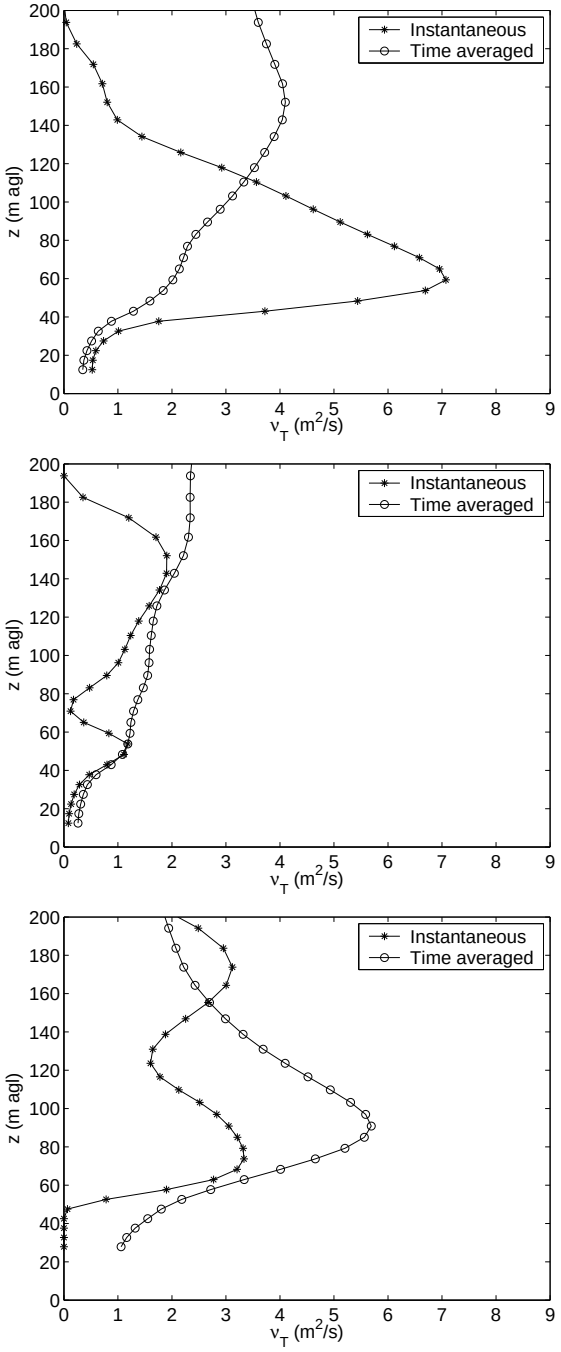

Figure 11: Profiles of the dynamic eddy viscosity from DRM-ADM0 results at the reference site (top), on the upslope of the hill (middle), in the lee of the hill (bottom).

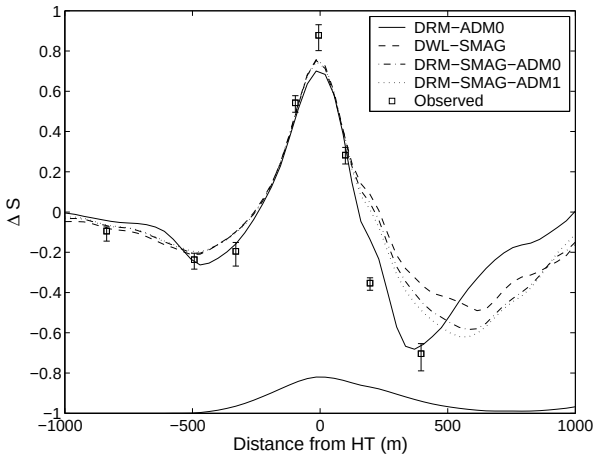

Figure 12: Comparisons of observed and simulated velocity speed-up along line A using DRM-ADM0, DWL-SMAG, DRM-SMAG-ADM0, and DRM-SMAG-ADM1 closures.

where the eddy viscosity is underpredicted. This hybrid approach augments the eddy viscosity near the wall and allowed the expected recirculation patterns to form in the lee of their hill. Figure 12 shows the wind speedup ratio along line A for a similar hybrid approach, where we use static Smagorinsky at the lowest six levels (chosen based on the curves in Figs. 11), and the dynamic Wong-Lilly eddy viscosity elsewhere (denoted DWL-SMAG). The predicted speedup is not as good as previous results from the DRM-ADM0 simulations, but the prediction of flow deceleration in the lee of the hill improves with increasing reconstruction (from DWL-SMAG to DRM-SMAG-ADM1).

All the dynamic models include the near-wall stress model introduced for neutral boundary simulations by Chow et al. (2004), using a proportionality factor $C_c = 0.5$ and a layer height $h_c = 4\Delta x$. This near-wall stress is intended to provide much of the "missing" stress near the wall, but it appears to be too little, as the hybrid approach is needed to stabilize the simulations. Increasing the proportionality factor means increasing the near-wall stress contribution.The greatest difference among the speedup curves is again in the lee of the hill, where increasing C_c prevents the wind from speeding up as quickly in the lee of the hill. The results with $C_c = 0.8$ look similar to those from DWL-SMAG (not shown), but the effect of the near-wall stress contribution is not enough to stabilize the simulations. Tests with DRM-ADM1 and $C_c = 0.8$ and even up to 0.95 failed.

5. CONCLUSIONS

Large-eddy simulations of flow over Askervein hill, an isolated hill in Scotland, were compared to the field observations of Taylor and Teunissen (1987). This flow is a challenging test for reconstruction turbulence models which gave improved results for neutral boundary layer flow over flat terrain. This is the first time, to our knowledge, that reconstruction (scale-similarity) or dynamic turbulence models have been applied to full-scale simulations of the atmospheric boundary layer over terrain.

Simulations with the lowest level of reconstruction (DRM-ADM0) are straightfoward and showed improvement for wind speedup-ratios over the hill, when compared to results from the standard TKE-1.5 model. Predictions of total turbulent kinetic energy were also improved using the DRM. Results were not as clear for the uw and vw stress components. Increased levels of reconstruction (beyond level 0) presented difficulties and required modification of the closure model near the ground. This was in part because the dynamic procedure underpredicts the stress near the wall over rough surfaces. While all of the simulations using reconstruction also included an enhanced near-wall stress model, this was not sufficient to prevent instabilities. We adopted the hybrid approach of Iizuka and Kondo (2003), using the static Smagorinsky model in the lowest levels near the wall and the dynamic approach above. The specification of this static Smagorinsky layer was based on profiles of the dynamic eddy viscosity, however, the appropriate transition level from static to dynamic requires further study. The results, though promising, show that problems with the behavior of closure models in this sensitive near-wall region of the flow have not been completely solved.

6. ACKNOWLEDGMENTS

The support of NSF Grant ATM-0073395 (Physical Meteorology Program: W.A. Cooper, Program Director) is gratefully acknowledged. Acknowledgment is also made to the National Center for Atmospheric Research, which is sponsored by NSF, for the computing time used in this research.

REFERENCES

Allen, T. and A. R. Brown, 2002: Large-eddy simulation of turbulent separated flow over rough hills. *Boundary-Layer Meteorology*, **102**, 177 – 198.

Besio, S., A. Mazzino, and C. F. Ratto, 2003: Local log-law-of-the-wall in neutrally-stratified boundary-layer flows. *Boundary-Layer Meteorology*, **107**, 115 – 42.

Bradley, E. F., 1980: An experimental study of the profiles of wind speed, shearing stress and turbulence at the crest of a large hill. *Quarterly Journal of the Royal Meteorological Society*, **106**, 101 – 23.

Brown, A., J. Hobson, and N. Wood, 2001: Large-eddy simulation of neutral turbulent flow over rough sinusoidal ridges. *Boundary-Layer Meteorology*, **98**, 411–441.

Castro, F. A., J. M. L. M. Palma, and A. S. Lopes, 2003: Simulation of the Askervein flow. Part 1: Reynolds averaged Navier-Stokes equations (k-epsilon turbulence model). *Boundary-Layer Meteorology*, **107**, 501 – 530.

Chow, F., 2004: *Subfilter-scale turbulence modeling for large-eddy simulation of the atmospheric boundary layer over complex terrain*. Ph.D. dissertation, Stanford University.

Chow, F. K., R. L. Street, M. Xue, and J. H. Ferziger, 2004: Explicit filtering and reconstruction turbulence modeling for large-eddy simulation of neutral boundary layer flow. *Journal of Atmospheric Sciences*, **submitted**.

Deardorff, J. W., 1980: Stratocumulus-capped mixed layers derived from a 3-dimensional model. *Boundary-Layer Meteorology*, **18**, 495 – 527.

Gullbrand, J. and F. K. Chow, 2003: The effect of numerical errors and turbulence models in large-eddy simulations of channel flow, with and without explicit filtering. *Journal of Fluid Mechanics*, **495**, 323 – 341.

Iizuka, S. and H. Kondo: 2003, Large eddy simulations of turbulent flow over complex terrain. *Proc. 11th International Conference on Wind Engineering, Vol. 2*, Texas, USA, 2689–2696.

Kim, H. G. and V. C. Patel, 2000: Test of turbulence models for wind flow over terrain with separation and recirculation. *Boundary-Layer Meteorology*, **94**, 5 – 21.

Klemp, J. and R. Wilhelmson, 1978: The simulation of three-dimensional convective storm dynamics. *Journal of Atmospheric Sciences*, **35**, 1070–1096.

Lavery, T., A. Bass, D. Strimaitis, A. Venkatram, B. Greene, P. Drivas, and B. Egan, 1982: EPA complex terrain model development: First milestone report - 1981. EPA-600/3-82-036, Environmental Protection Agency.

Mason, P. J. and J. C. King, 1985: Measurements and predictions of flow and turbulence over an isolated hill of moderate slope. *Quarterly Journal of the Royal Meteorological Society*, **111**, 617 – 40.

Moeng, C.-H., 1984: A large-eddy-simulation model for the study of planetary boundary-layer turbulence. *Journal of Atmospheric Sciences*, **41**, 2052–2062.

Raithby, G. D., G. D. Stubley, and P. A. Taylor, 1987: The Askervein Hill project: a finite control volume prediction of three-dimensional flows over the hill. *Boundary-Layer Meteorology*, **39**, 247 – 67.

Salmon, J. R., H. W. Teunissen, R. E. Mickle, and P. A. Taylor, 1988: The Kettles Hill project: field observations, wind-tunnel simulations and numerical model predictions for flow over a low hill. *Boundary-Layer Meteorology*, **43**, 309 – 43.

Stolz, S., N. Adams, and L. Kleiser, 2001: An approximate deconvolution model for large-eddy simulation with application to incompressible wall-bounded flows. *Physics of Fluids*, **13**, 997–1015.

Strimaitis, D., A. Venkatram, B. Greene, S. Hanna, S. Heisler, T. Lavery, A. Bass, and B. Egan, 1982: EPA complex terrain model development: Second milestone report - 1982. EPA-600/3-83-015, Environmental Protection Agency.

Taylor, P. and H. Teunissen, 1985: The Askervein hill project: Report on the September/October 1983 main field experiment. Report msrb-84-6, Atmospheric Environment Service, Downsview, Ontario.

Taylor, P. A. and H. W. Teunissen, 1987: The Askervein Hill project: overview and background data. *Boundary-Layer Meteorology*, **39**, 15 – 39.

Walmsley, J. L. and P. A. Taylor, 1996: Boundary-layer flow over topography: impacts of the Askervein study. *Boundary-Layer Meteorology*, **78**, 291 – 320.

Wong, V. C. and D. K. Lilly, 1994: A comparison of two dynamic subgrid closure methods for turbulent thermal-convection. *Physics of Fluids*, **6**, 1016 – 1023.

Xue, M., K. Droegemeier, V. Wong, A. Shapiro, and K. Brewster, 1995: *ARPS Version 4.0 User's Guide*. Center for Analysis and Prediction of Storms, University of Oklahoma, Norman, OK.

Xue, M., K. K. Droegemeier, and V. Wong, 2000: The advanced regional prediction system (ARPS): A multi-scale nonhydrostatic atmospheric simulation and prediction model. Part I: Model dynamics and verification. *Meteorology and Atmospheric Physics*, **75**, 161–193.

Xue, M., K. K. Droegemeier, V. Wong, A. Shapiro, K. Brewster, F. Carr, D. Weber, Y. Liu, and D. Wang, 2001: The advanced regional prediction system (ARPS): A multi-scale nonhydrostatic atmospheric simulation and prediction tool. Part II: Model physics and applications. *Meteorology And Atmospheric Physics*, **76**, 143–165.